Original Article

A closer look at the structure and gamma-ray shielding properties of newly designed boro -tellurite glasses reinforced by bismuth (III) oxide

Hammam Abdurabu Thabit [a, *], Abd Khamim Ismail [a, **], N.N. Yusof [b], M.I. Sayyed [c, d], K.G. Mahmoud [e], I. Abdullahi [a, f], S. Hashim [a]

[a] Department of Physics, Universiti Teknologi Malaysia, 81310, Johor Bahru, Malaysia
[b] School of Physics, Universiti Sains Malaysia, 11800, USM, Penang, Malaysia
[c] Department of Physics, Faculty of Science, Isra University, Amman, 11622, Jordan
[d] Department of Nuclear Medicine Research, Institute for Research and Medical Consultations (IRMC), Imam Abdulrahman bin Faisal University, P.O Box 1982, Dammam 31441, Saudi Arabia
[e] Ural Federal University, St. Mira, 19, 620002, Yekaterinburg, Russia
[f] Physics Department, Federal University, Gusau, Zamfara State, Nigeria

ARTICLE INFO

ABSTRACT

This work presents the synthesis and preparation of a new glass system described by the equation of (70-x) $B_2O_3-5TeO_2 -20SrCO_3-5ZnO -xBi_2O_3$, x = 0, 1, 5, 10, and 15 mol. %, using the melt quenching technique at a melting temperature of 1100 °C. The photon-shielding characteristics mainly the linear attenuation coefficient (LAC) of the prepared glass samples were evaluated using Monte Carlo (MC) simulation N-particle transport code (MCNP-5) at gamma-ray energy extended from 59 keV to 1408 keV emitted by the radioisotopes Am-241, Ba-133, Cs-137, Co-60, Na-22, and Eu-152. Furthermore, we observed that the Bi_2O_3 content of the glasses had a significantly stronger impact on the LAC at 59 and 356 keV. The study of the lead equivalent thickness shows that the performance of fabricated glass sample with 15 mol.% of Bi_2O_3 is four times less than the performance of pure lead at low gamma photon energy while it is enhanced and became two times lower the perforce of pure lead at high energy. Therefore, the fabricated glasses special sample with 15 mol.% of Bi_2O_3 has good shielding properties in low, intermediate, and high energy intervals.

© 2023 Korean Nuclear Society, Published by Elsevier Korea LLC. This is an open access article under the CC BY-NC-ND license (http://creativecommons.org/licenses/by-nc-nd/4.0/).

1. Introduction

In recent decades, there has been an increased need for radiation shielding materials, which has attracted appropriate care in the effort to lessen the risks that radiation poses to living organisms. Employees who might be exposed to ionizing radiation can be seriously harmful to them owing to being impacted perhaps by unnecessary exposures during the usage of various modern techniques. This is one of the many dangers that exist with advances in technology nuclear and radioactive technologies. A wide variety of materials, beginning with rocks, concrete, glass, ceramic, clay brick, slag, iron, and polymer with various additions, have been developed to be used in the field of radiation shielding [1—10].

One of the most significant parts of radiological protection is the use of high-density compounds, which increases the amount of radiation absorbed. This is done with the goal of reducing the amount of radiation to which an individual is exposed. In order to fulfill this growing demand for transparent protective materials, unique glass systems have been developed as radiation shielding components that may be used in a variety of compositions. Besides the enhancement of shielding properties of the developed glass systems, suitable optical and physical characteristics should be considered for the developed glass systems. The optical, physical, and structural attributes of the glass are determined by the primary elements present in the glass composition, such as borate, phosphate, tellurite, and silicate [11—15].

Furthermore, the radiation shielding characteristics of glasses

* Corresponding author.
** Corresponding author.
E-mail addresses: hammam.tha@gmail.com, a.abdurabu@utm.my (H.A. Thabit), khamim@utm.my (A.K. Ismail).

are strongly dependent on the glass density and composition of the sample where dense glass is better than light ones for gamma-ray protection applications.

Boro-tellurite glass hosts combines the features of borates and tellurites thus, they are characterized by superb properties of reduced melting temperature, thermal stability, good optical transparency, low phonon energy, appreciable glass forming ability, high chemical durability, rare earth solubility, and wide optical transmission window [16–19]. Hence, they are widely studied glass material [20–22].

Currently, numerous glasses have been researched as a potentially superior shielding material by numerous researchers, which tested the potential applications of these glasses by a combination of practical, analytical, and computing methodologies [23–26]. Different research groups have researched the impact of using heavy metals as a replacement for Pb in radiation protection glass [27,28]. In addition, several studies have investigated the low energy shielding range for several glasses containing some heavy elements added to the glass systems. These studies concluded that the addition of further heavy metal oxides (HMO) will improve the density of the sample, which, in turn, will enhance the sample's capacity to attenuate photons [29]. Minimizing the mean free path (MFP) is another method for estimating the radiation shielding parameters. Glasses that were produced using the melt quenching technique showed that adding some kinds of dense materials will decrease the MFP, which led to improvements in the radiation protection ability of the prepared glasses [30–33].

The present work aims to fabricate a new boro-tellurite glass system consisting of B_2O_3, TeO_2, $SrCO_3$, ZnO, and Bi_2O_3 chemical compounds. The effect of partial replacement for B_2O_3 by the dense Bi_2O_3 on the structural, physical, and gamma-ray shielding properties were investigated.

2. Materials and methods

2.1. Glass preparation

A series of glasses (70-x) B_2O_3–5TeO_2 –20$SrCO_3$–5ZnO –xBi_2O_3, x = 0%, 1%, 5%, 10%, and 15% mol have been synthesized by melt quenching technique. The chemical raw materials of B_2O_3 (2.46 g/cm^3), TeO_2 (5.67 g/cm^3), $SrCO_3$ (3.5 g/cm^3), ZnO (5.61 g/cm^3), and Bi_2O_3 (8.9 g/cm^3), were utilized in powder form with high purity (99.99%, Sigma-Aldrich). The chemical powders were weighed with a high accuracy level ($\pm$0.001 mg) using an electronic balance and carefully combined with roughly 10 g of raw materials in each glass specimen. All the samples were carefully mixed to produce a uniform composition using the agate mortar. The powder was melted for 60 min at 1100 °C in an aluminum crucible to stabilize its homogeneity and eliminate air bubbles. The molten glass was immediately poured wisely on the stainless-steel plate prepared inside the annealing furnace and annealed at 400 °C for 24 h, then cooled gradually to reduce thermal stress and strain induced by the heat treatment. The produced glasses were labeled as S1, S2, S3, S4, and S5 for x = 0, 1, 5, 10, and 15 mol.% of Bi_2O_3. The methodical and sequential steps that were taken in order to prepare the sample are shown in Fig. 1. The density (ρ) of the obtained glass specimens was estimated using the traditional technique of Archimedes using toluene as the liquid medium, and the molar volume (V_m) was calculated and listed in Table 1.

The density (ρ) was calculated using Archimedes' principle using the relation:

$$\rho = \frac{W_a}{W_a - W_b} \times \rho_T \tag{1}$$

where W_a, W_b, and ρ_T are the weights of the glass sample in air, toluene, and the density of toluene ($\approx$0.86 g/cm^3), respectively.

The molar volume (V_m) was calculated using the relation:

$$V_m = \frac{M_w}{\rho} \tag{2}$$

where M_w and ρ are the molecular weight and the density of the glass sample, respectively.

2.2. Structural investigation

The influence of the partial replacement of B_2O_3 compounds by Bi_2O_3 on the color of the fabricated glass was illustrated in Fig. 1. The color of the fabricated samples was changed depending on the composition of glass samples, where increasing the Bi_2O_3 concentration causes a slight change in the visual coloration from colorless and transparent to light brown. The mentioned transformation in the glass colors is attributed to the reduction of Bi^{3+} ions to bismuth metal (Bi) during the melting process [34].

After that, a specimen of glass was crushed into fine powder form to investigate the structural properties through X-Ray Diffraction (XRD). Fig. 2 reveals the synthesized XRD patterns of these glasses as labeled from S1 to S5. The study was conducted between 20° and 80° angles. The results appeared to be broad humps peaks which confirm the glasses synthesized have an amorphous [3].

The measurements of the fabricated glasses density showed an enhancement in the sample's density from 2.90 t0 4.28 g/cm^3 as well as an increase in the molar volume increased from 31.15 to 34.95 cm^3/mol with raising the Bi_2O_3 concentration between 0 and 15 wt%, as illustrated in Table 1.

The variation in the glass's density can be attributed to the atomic mass of elements constituting the fabricated glass. Therefore, the partial replacement of a low molecular weight compound (i.e., B_2O_3 with a molecular weight of 69.63 g/mol) by a higher molecular weight compound Bi_2O_3 (336.48 g/mol) causes an increase in the molecular weight of the fabricated glass due to the increase in the Bi^{3+} ions in the glass. The increase in samples density and molecular mass is reflected in the molar volume of the fabricated glasses where the molar volume increased from 31.15 to 34.95 cm^3/mol with raising the Bi^{3+} ions in the fabricated samples.

2.3. Radiation shielding evaluations

The Monte Carlo simulation N-particle transport code (MCNP-5) [35] was applied to evaluate the average track length (ATL) of gamma-photons inside the fabricated glass samples. The input file that describes the simulation geometry consists of many cards, such as cell, surface, material, source, importance, and physical cards can be seen in Fig. 3. The cell is the main unit to build the geometry, where each unit in the geometry should be represented by a cell. The surface card is the card that is responsible to define the boundaries and dimensions of each cell. Moreover, the material card contains the synthesized glass material's elemental chemical composition and density. The source card (SDEF card) contains the source energy, position, emission direction, source distribution, and probability. In the present simulation, the cutoff card was set to stop the photon emission after 10^6 historical and the tally card was
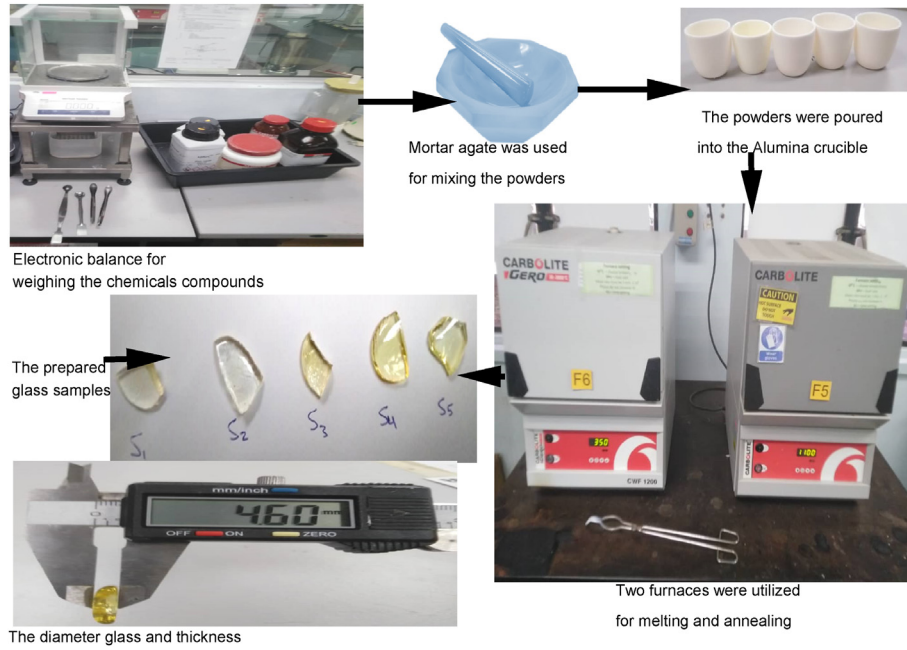
Fig. 1. The graphic shows the steps and procedure for the prepared glass.

Table 1
Density, molar volume and the Weight fraction mol% of compounds for the glasses (70-x) B_2O_3−5TeO_2 −20$SrCo3$ −5ZnO −xBi_2O_3: $0 \leq x \leq 15$ *mol*.%.

Component	Composition Mol%	Density (g/cm³)	Molar volume cm³/mol
70B_2O_3−5TeO_2−20$SrCo_3$ 5-ZnO- 0Bi_2O_3	90.30	2.90	31.15
69B_2O_3−5TeO_2−20$SrCo_3$-5 ZnO−1Bi_2O_3	94.27	3.00	31.48
65B_2O_3−5TeO_2−20$SrCo_3$−5ZnO− 5Bi_2O_3	110.13	3.41	32.28
60B_2O_3−5TeO_2−20$SrCo_3$-5 ZnO− 10Bi_2O_3	129.94	3.92	33.13
55B_2O_3−5TeO_2−20$SrCo_3$-5 ZnO− 15Bi_2O_3	149.76	4.28	34.95

chosen to be F4 to estimate the average track length of gamma photons (ATL). Moreover, the database used to provide the simulation code with the cross-section database is ENDF/B-VI8. After running the simulation, the ATL for gamma photons was arranged in an output file. These output files illustrate that the relative error in the simulation process at all γ-photon energies is in the range of ±1 [36,37].

After recording the ATL for the fabricated samples at the selected γ-photon energies between 59 and 1408 keV, the ATL values were used to evaluate the critical shielding parameters such as linear attenuation coefficient (μ, cm^{-1}), half value layer ($\Delta_{0.5}$, cm), lead equivalent thickness (Δ_{eq}, cm), transmission factor (TF, %), and radiation protection efficiency (RPE, %) thought the following equations [38].

$$\mu \left(cm^{-1} \right) = \frac{1}{x} \ln\left(\frac{I_o}{I}\right) \tag{3}$$

I_o and I, refer to the total emitted photon number and penetrated photon number, respectively. The thickness required to absorb half of applied γ-photons is known as the half-value thickness ($\Delta_{0.5}$, cm), where it is reversely proportional to the μ value according to eq (4).

$$\Delta_{0.5} \ (cm) = \frac{\ln(2)}{\mu} \tag{4}$$

Moreover, the transmission factor (TF) is related to I and I_0 via equation (5):

$$TF \ (\%) = \frac{I}{I_o} \times 100 \tag{5}$$

The radiation protection efficiency is given by:

$$RPE \ (\%) = \frac{(I_o - I)}{I_o} \times 100 \tag{6}$$

3. Results and discussion

In Fig. 4, the linear attenuation coefficient, or LAC, for the newly prepared glasses was simulated and graphed against gamma-ray photon energy using Monte Carlo (MC) simulations. The theoretical values calculated from XCOM, and the simulated LAC from the MC simulations had high agreements with each other at all tested energies for all the tested samples. A small difference within a range of ±2.3 was observed between the simulated and XCOM's LAC values.

The dependence between the linear attenuation coefficients of the glasses and their Bi_2O_3 content is plotted in Fig. 5. The results were plotted at four varying energies, and at all of these LAC increased linearly with Bi_2O_3. In other words, increasing the concentration of Bi_2O_3 causes an improvement in the LAC. The slope of the coefficients at 59 and 356 keV is much higher than at higher energies, such as 661−1408 keV. This result indicates that the Bi_2O_3 content in the glasses has a much greater effect on the LAC at 59
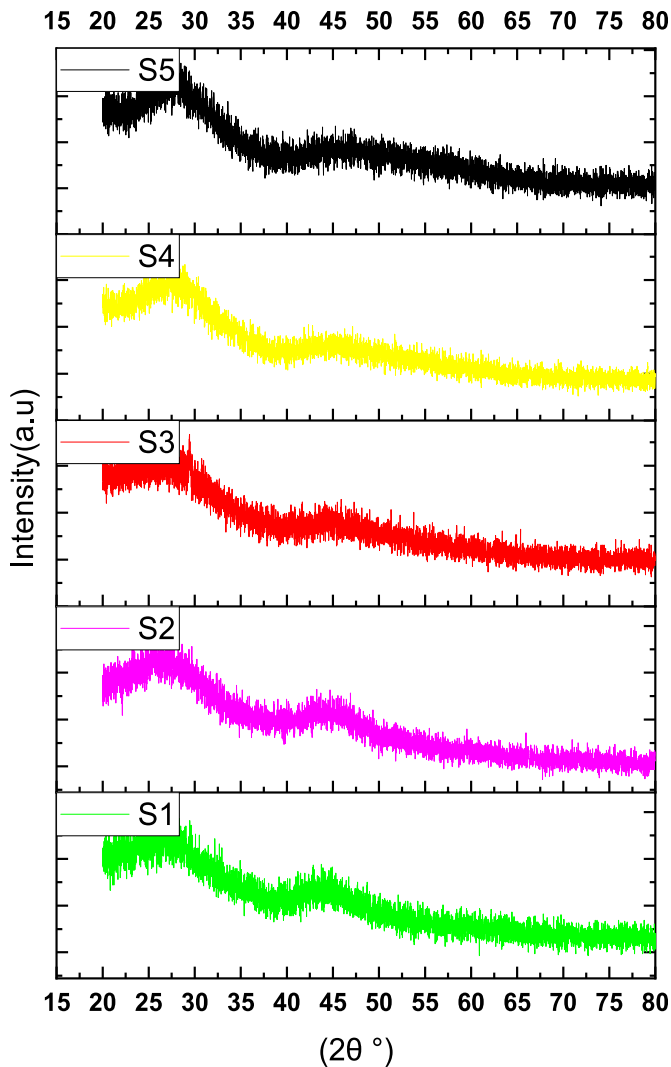
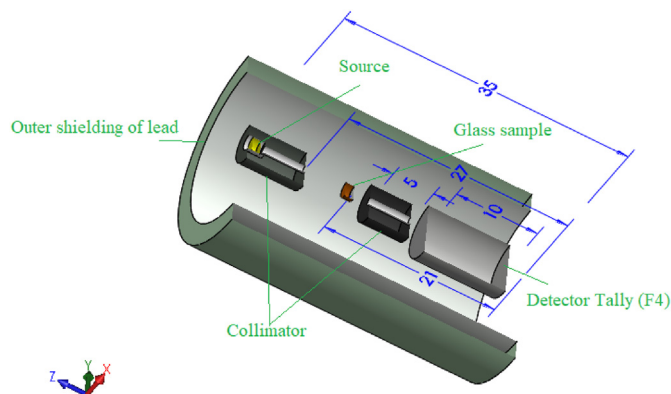**Fig. 2.** The XRD of the synthesized glass samples.

Fig. 3. The MCNP-3 geometry as illustrated in the created input file.

Fig. 4. Variation of the linear attenuation coefficient (μ, cm^{-1}) versus the emitted g-photon energy.
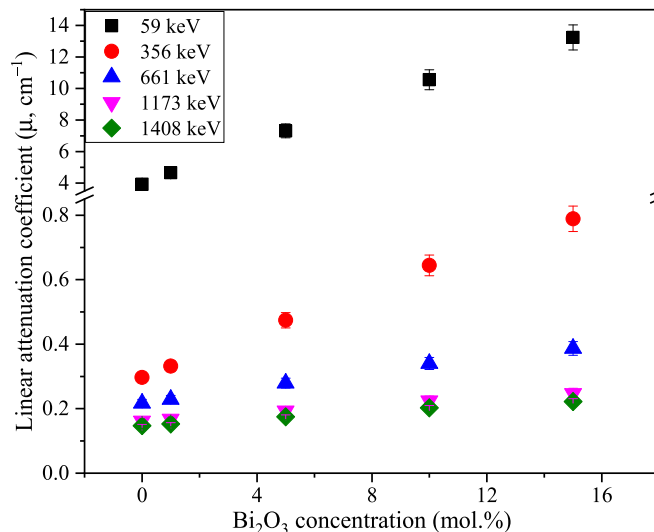
Fig. 5. Dependence of the linear attenuation coefficient (μ, cm^{-1}) on the Bi$_2$O$_3$ inserted ratio.

and 356 keV while having a less but still meaningful effect at higher energies [39]. This trend occurs attributed to the relationship between the atomic number and the cross-section of the Photoelectric effect, which is dominant at 59 and 356, and the Compton scattering effect, which is dominant at 661−1408 keV. In addition, this figure als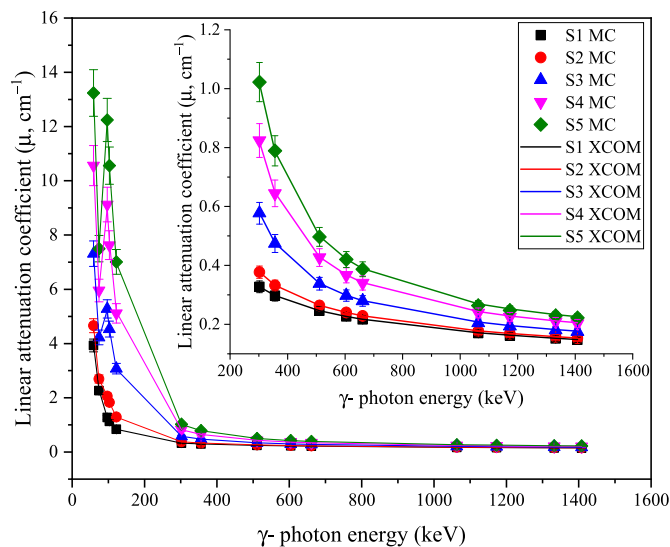o demonstrates that increased photon energy lowers the LAC of the glasses for all concentrations. For example, the LAC of the S3 glass drops from 7.31 cm^{-1} at 59 keV to 0.28 cm^{-1} at 661 keV and 0.18 cm^{-1} at 1408 keV. This trend indicates that higher photons have an easier time penetrating through the prepared glasses than lower energy photons.

The μ values for the fabricated boro-tellurite glasses reinforced Bi$_2$O$_3$ compound (S1−S5) at a gamma photon energy of 661 keV were compared to the μ values for previously similar published glasses doped Bi$_2$O$_3$ [40,41], as illustrated in Fig. 6. The comparison depicts that the μ values for the present work glasses are 0.217, 0.229, 0.279, 0.349, and 0.387 cm^{-1} for samples S1, S2, S3, S4, and S5, respectively. The previously mentioned results showed that the sample S1 has the lowest μ values in the comparison while S2 and S3 have μ values comparable to those reported for samples BBBi0, BBBi2.5, BBBi5, EBiBY0.05, and EBiBY0.1 with μ values of 0.240, 0.247, and 0.255, 0.291, and 0.298 cm^{-1}, respectively. Moreover, the fabricated samples S4 and S5 have μ values higher than BBBi0, BBBi2.5, BBBi5, EBiBY0.05, EBiBY0.1, EBiBPY0.25, EBiBPY0.5,
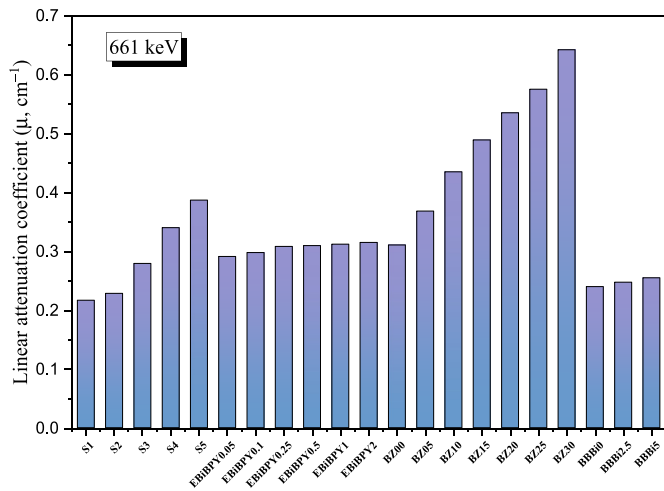
Fig. 6. Comparison between the fabricated glasses' μ values and those of previously reported glasses reinforced with Bi_2O_3 compounds.

EBiBPY1, and EBiBPY2, while S4 and S5 μ values are comparable to previously published samples BZ00 and BZ05 with μ values of 0.311 and 0.368 cm^{-1}. Fig. 6 depicts that the fabricated samples have μ values lower than that reported for samples BZ10, BZ15, BZ20, BZ25, and BZ30 with μ values of 0.435, 0.489, 0.535, 0.575, and 0.642 cm^{-1}, respectively. The reason for high μ values for the BZ samples is the high Bi_2O_3 content which reaches more than 30 mol % of the glass composition, which is reflected in the glass density where the BZ glasses have density varied between 4.1 and 7.1 g/cm^3 for glasses BZ00- BZ30, respectively.

Fig. 7 shows the effect of the Bi_2O_3 doping ratio on the half-value thickness ($\Delta_{0.5}$, cm) and mean free path (λ, cm) of the fabricated glass samples at 59 and 661 keV. Both parameters have a decreasing trend with Bi_2O_3. For example, at 59 keV, the $\Delta_{0.5}$ are equal to 0.18 cm at 0 mol% Bi_2O_3, 0.09 cm at 10 mol% Bi_2O_3, and 0.05 at 15 mol% Bi_2O_3. Meanwhile, λ values at the same energy equal 0.25, 0.14, and 0.08 cm at the same Bi_2O_3 concentrations. This trend means that the more Bi_2O_3 is added to the glasses, the smaller or less thick the samples need to be adequately used in radiation shielding applications. The figure also reveals that both the $\Delta_{0.5}$ and the λ increase with energy. At 0 mol% Bi_2O_3, $\Delta_{0.5}$ increases from
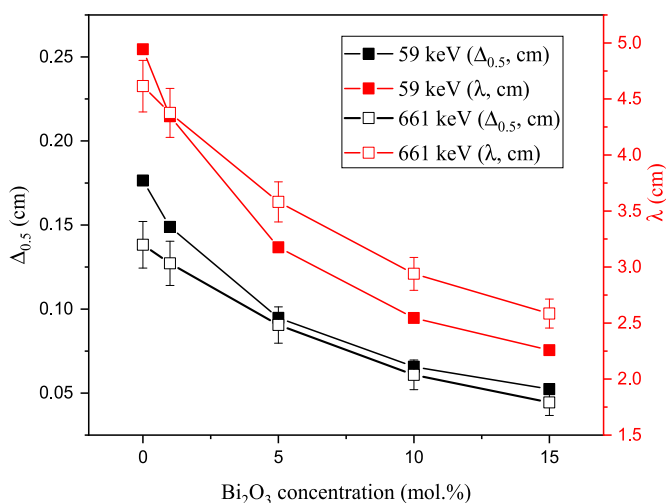
0.18 cm at 59 keV to 3.20 cm at 661 keV, while λ increases from 0.25 cm to 4.61 at the same respective energies. These values demonstrate that the thickness of the glasses needs to increase if the material needs to absorb higher energy photons while maintaining the same level of attenuation.

The lead equivalent thickness or Δ_{eq} of the fabricated samples are graphed against gamma-ray photon energies in Fig. 8. The Δ_{eq} of the samples generally decreases with increasing photon energy, except for a spike in values around 97 keV. For example, S2's Δ_{eq} is equal to 33.0 cm at 97 keV, 9.8 cm at 356 keV, 5.5 cm at 661 keV, and 4.0 cm at 1408 keV. The figure also shows that the Δ_{eq} is inversely related to the Bi_2O_3 content in the glasses. In other words, the S5 glass has the greatest Bi_2O_3 content and the lowest Δ_{eq}. This is most evidently seen at lower energies, where the amount of Bi_2O_3 in the glasses tends to have a greater impact on their shielding ability. More specifically, at 302 keV, S1 has a Δ_{eq} of 13.8 cm, while S5 has a Δ_{eq} of 4.4 cm. This trend reinforces the conclusion that increasing the Bi_2O_3 content in the glasses leads to a better shielding ability for radiation shielding applications.

Fig. 9 illustrates the effect between the Bi_2O_3 doping ratio and the lead equivalent thickness Δ_{eq} of the fabricated glass samples. Increasing the Bi_2O_3 concentration leads to a decrease in Δ_{eq}, which means that adding more Bi_2O_3 into the glasses leads to a better shielding ability. This decrease in Δ_{eq} values means that the shielding ability of the prepared samples approaches the equivalent attenuation capability of lead, making the glass more effective. At high concentrations such as at 15 mol% Bi_2O_3, the Δ_{eq} values range from 2.8 to 4.2 cm, which is much lower compared to at 0 mol% Bi_2O_3, where they range from 4.5 to 15.1 cm. The mentioned results showed that the performance of lead material is four times higher than the fabricated glass sample S5 (with Bi_2O_3 concentration of 15 mol.%) at low gamma photon energy while at intermediate and high energy the performance of the fabricated glass sample S5 enhanced and became only two times less than the performance of pure lead. Thus, the fabricated glass samples (especially S5) are considered a suitable candidate for photon shielding at low, intermediate, and high gamma photon energies.

The effect of the Bi_2O_3 concentration on the transmission factor (TF) and the radiation protection efficiency (RPE) of the newly prepared samples is graphed in Fig. 10 at 356 and 661 keV. At both energies, TF decreases as more Bi_2O_3 is added to the glasses, while RPE increases with more Bi_2O_3. For example, at 356 keV, the TF
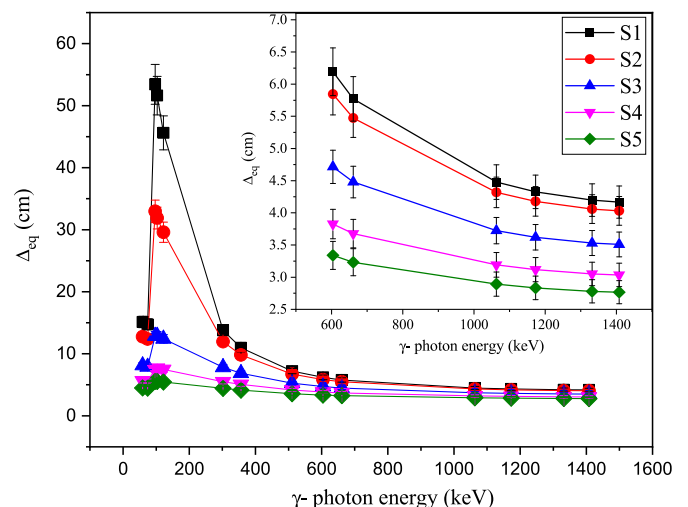

Fig. 7. Effect of Bi_2O_3 doping ratio on both half value thickness (Δ0.5, cm) and mean free path (λ, cm) of the fabricated glass samples.

Fig. 8. Dependence of the fabricated samples' lead equivalent thickness (Δ_{eq}, cm) on the emitted γ-photon energy.
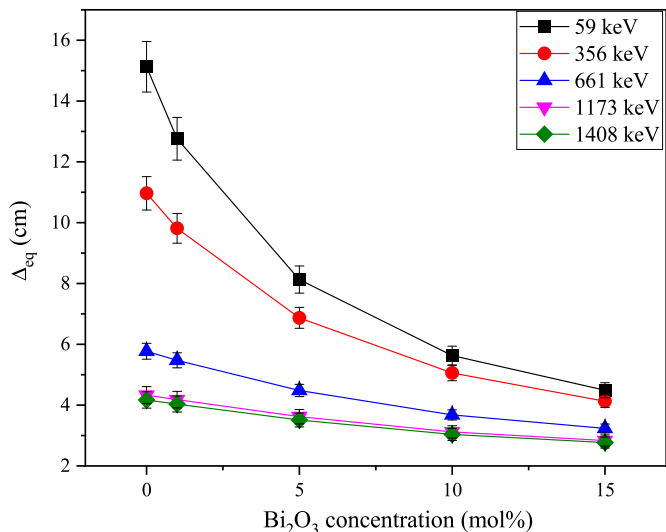
Fig. 9. Effect of Bi$_2$O$_3$ doping ratio on the lead equivalent thickness (Δ_{eq}, cm) for the fabricated samples.
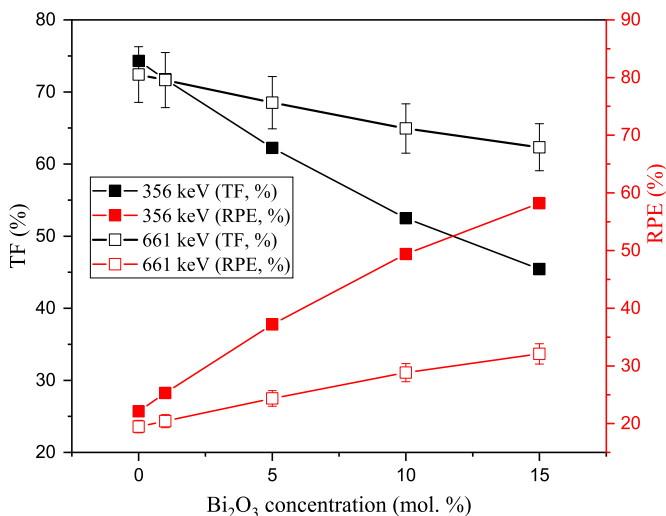

Fig. 10. Effect of Bi$_2$O$_3$ doping ratio on both transmission factor (TF, %) and radiation protection efficiency (RPE, %) of the fabricated samples.

Fig. 11. Dependence of both transmission factor (TF, %) and radiation protection efficiency (RPE, %) on the fabricated glass thickness at γ-photon energy of 604 keV.

values decrease from 74.3% to 71.7%, 62.2%, 52.5%, and 45.4% for 0, 1, 5, 10, and 15 Bi$_2$O$_3$ mol%, while the RPE values are equal to 25.7%, 28.3%, 37.8%, 47.5%, and 54.6%, for the same respective concentrations. Both results show that a greater Bi$_2$O$_3$ doping ratio correlates with a better shielding ability. Comparing the energies themselves, the TF values generally increase with greater energy, and the RPE values decrease with energy. For instance, at 5 mol% Bi$_2$O$_3$, the TF values are equal to 66.2% at 356 keV and 75.6% at 661 keV, and the RPE values are equal to 37.8% and 24.4% for the same respective energies. Thus, more photons can penetrate through the samples when they have higher energies, while lower energy photons can be observed by the glasses.

The TF and RPE's dependence on the glasses' thickness at 604 keV is shown in Fig. 11. The figure shows the TF and RPE of S1 and S4 to also compare the effect of the Bi$_2$O$_3$ content on these parameters. First, increasing the thickness of the glasses both lowers TF and raises RPE. More specifically, S1's TF drops from 94.5% to 71.2% at a thickness of 0.25 cm at 1.5 cm, respectively, while its RPE increases from 5.5%–28.8% at the same thicknesses. Similar
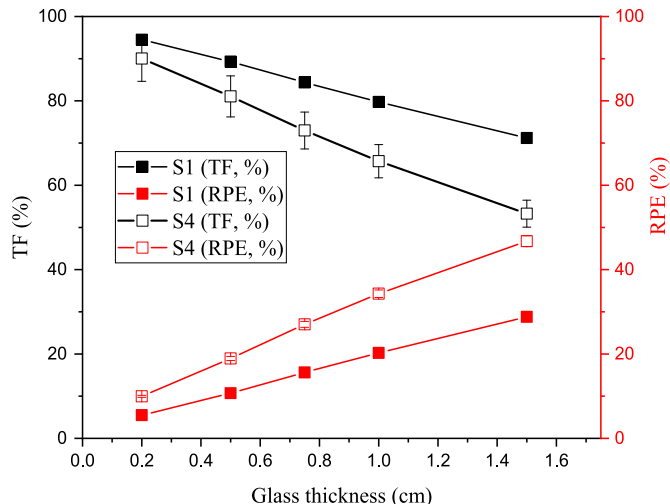
trends can be observed for S4. Therefore, if space is available, increasing the thickness of the glasses greatly reduces the number of photons that can penetrate through the sample, which can especially help against higher energy photons. Between S1 and S4, S4 has a lower TF and a higher RPE at all thicknesses, but this difference increases with increasing thickness. Therefore, having a greater Bi$_2$O$_3$ concentration also helps increase the benefit gained from an increase in glass thickness.

4. Conclusion

A glass system with a chemical concentration of (70-x) B$_2$O$_3$−5TeO$_2$−20SrCO$_3$−5ZnO −xBi$_2$O$_3$, x = 0, 1, 5, 10, and 15 mol. % was fabricated in order to determine the influence of the partial replacement of the B$_2$O$_3$ by Bi$_2$O$_3$ compounds in the fabricated system. The first look at the fabricated samples shows a slight change in the color of the fabricated glasses where the sample colors became light brown with increasing the Bi$_2$O$_3$ concentration in the fabricated glass. After that, the XRD pattern affirms the amorphous phase of the fabricated glasses. Moreover, the experimental measurements for the glass density show an increase by a factor of 47.8% by raising the Bi$_2$O$_3$ concentration between 0 and 15 mol.%. This increase affirms also the replacement of light B$_2$O$_3$ by a heavy Bi$_2$O$_3$ compound. The Monte Carlo simulation was utilized to estimate the γ-ray shielding parameter for the fabricated samples in the energy interval between 59 and 1408 keV. The obtained results depict a high increase in the linear attenuation coefficient at low gamma energy due to the predominant photoelectric interaction. For example, at γ-photon energy of 59 keV, the linear attenuation coefficient was enhanced by a factor of 237% by raising the Bi$_2$O$_3$ concentration to 15 mol.%. The enhancement of the linear attenuation coefficient decreased with increasing the γ-photon energy due to an increase in the penetration power of the γ-photons with raising the photon energy. The enhancement ratio in the linear attenuation coefficient values reduced to 50% at γ-photon energy of 1408 keV. Then the lead equivalent thickness was evaluated for the fabricated study where it decreased from 4.2 cm to 2.8 cm by raising the Bi$_2$O$_3$ concentration between 0 and 15 mol.%, respectively. The small equivalent thickness for the fabricated glasses (especially for the S5 sample) showed a high-performance reach of 35% compared to the performance of pure lead at a high γ-photon energy of 1408 keV. The mentioned results showed that

the fabricated glass S5 has a suitable shielding property to be applied in radiation protection applications.

Declaration of competing interest

The authors declare that they have no known competing financial interests or personal relationships that could have appeared to influence the work reported in this paper.

Acknowledgments

References

[1] S.A. Abo-El-Enein, F.I. El-Hosiny, S.M.A. El-Gamal, M.S. Amin, M. Ramadan, Gamma radiation shielding, fire resistance and physicochemical characteristics of Portland cement pastes modified with synthesized Fe2O3 and ZnO nanoparticles, Construct. Build. Mater. 173 (2018) 687–706, https://doi.org/10.1016/j.conbuildmat.2018.04.071.

[2] M. Dong, X. Xue, H. Yang, Z. Li, Highly cost-effective shielding composite made from vanadium slag and boron-rich slag and its properties, Radiat. Phys. Chem. 141 (2017) 239–244, https://doi.org/10.1016/j.radphyschem.2017.07.023.

[3] Shams A.M. Issa, Mahmoud Ahmad, H.O. Tekind, Yasser B. Saddeek, M.I. Sayyed, Effect of Bi₂O₃ content on mechanical and nuclear radiation shielding properties of Bi₂O₃-MoO₃-B₂O₃-SiO₂-Na₂O-Fe₂O₃ glass system, Results Phys. 13 (2019) 102165.

[4] M.A. Khalaf, C.C. Ban, M. Ramli, The constituents, properties and application of heavyweight concrete: a review, Construct. Build. Mater. 215 (2019) 73–89, https://doi.org/10.1016/j.conbuildmat.2019.04.146.

[5] C.v. More, Z. Alsayed, MohamedS. Badawi, AbouzeidA. Thabet, P.P. Pawar, Polymeric composite materials for radiation shielding: a review, Environ. Chem. Lett. 19 (2021) 2057–2090, https://doi.org/10.1007/s10311-021-01189-9.

[6] A. Levet, E. Kavaz, Y. Özdemir, An experimental study on the investigation of nuclear radiation shielding characteristics in iron-boron alloys, J. Alloys Compd. 819 (2020), 152946, https://doi.org/10.1016/j.jallcom.2019.152946.

[7] S.F. Olukotun, S.T. Gbenu, F.I. Ibitoye, O.F. Oladejo, H.O. Shittu, M.K. Fasasi, F.A. Balogun, Investigation of gamma radiation shielding capability of two clay materials, Nucl. Eng. Technol. 50 (2018) 957–962, https://doi.org/10.1016/j.net.2018.05.003.

[8] Y.S. Rammah, A.S. Abouhaswa, M.I. Sayyed, H.O. Tekin, R. El-Mallawany, Structural, UV and shielding properties of ZBPC glasses, J Non-Cryst. Solids 509 (2019) 99–105.

[9] I.S. Mahmoud, Shams A.M. Issa, Yasser B. Saddeek, H.O. Tekin, Ozge Kilicoglu, T. Alharbi, M.I. Sayyed, T.T. Erguzel, Reda Elsaman, Gamma, neutron shielding and mechanical parameters for lead vanadate glasses, Ceram. Int. 45 (2019) 14058–14072.

[10] R.A. Bantan, M.I. Sayyed, K.A. Mahmoud, Application of experimental measurements, Monte Carlo simulation and theoretical calculation to estimate the gamma ray shielding capacity of various natural rocks, Prog. Nucl. Energy. 126 (2020) 103405.

[11] A.S. Abouhaswa, E. Kavaz, Bi2O3 effect on physical, optical, structural and radiation safety characteristics of B2O3Na2O-ZnO CaO glass system, J. Non-Cryst. Solids 535 (2020), 119993, https://doi.org/10.1016/j.jnoncrysol.2020.119993.

[12] M. Rajesh, E. Kavaz, B. D.P.R, Photoluminescence, radiative shielding properties of Sm3+ ions doped fluoroborosilicate glasses for visible (reddish-orange) display and radiation shielding applications, Mater. Res. Bull. 142 (2021), 111383, https://doi.org/10.1016/j.materresbull.2021.111383.

[13] M.S. Al-Buriahi, Y.S. Rammah, Electronic polarizability, dielectric, and gamma-ray shielding properties of some tellurite-based glasses, Appl. Phys. Mater. Sci. Process 125 (2019) 1–9, https://doi.org/10.1007/s00339-019-2976-z.

[14] M.T. Islam, R.M. Felfel, E.A.A. Neel, D.M. Grant, I. Ahmed, K.M.Z. Hossain, Bioactive calcium phosphate–based glasses and ceramics and their biomedical applications: a review, J. Tissue Eng. 8 (2017), https://doi.org/10.1177/2041731417719170.

[15] Y. Al-Hadeethi, M.I. Sayyed, Radiation attenuation properties of Bi2O3−Na2O− V2O5− TiO2−TeO2 glass system using Phy-X / PSD software, Ceram. int. 46 (2020) 4795–4800.

[16] I. Abdullahi, S. Hashim, S.K. Ghoshal, L. Sa'adu, Modified structure and spectroscopic characteristics of Sm3+/Dy3+ co-activated barium-sulfur-telluro-borate glass host: role of plasmonic gold nanoparticles inclusion, Opt Laser. Technol. 132 (2020), 106486, https://doi.org/10.1016/j.optlastec.2020.106486.

[17] R.A.A. Silva, N.F. Dantas, R.F. Muniz, A.M.O. Lima, F. Pedrochi, A. Steimacher, M.J. Barboza, Optical and spectroscopic properties of Er3+/Yb3+ co-doped calcium borotellurite glasses, J. Lumin. 251 (2022), 119239, https://doi.org/10.1016/j.jlumin.2022.119239.

[18] O. Agar, E. Kavaz, E.E. Altunsoy, O. Kilicoglu, H.O. Tekin, M.I. Sayyed, T.T. Erguzel, Nevzat Tarhan, Er2O3 effects on photon and neutron shielding properties of TeO2-Li2O-ZnONb2O5 glass system, Results Phys. 13 (2019) 102277.

[19] M.I. Sayyed, A. Kumar, B. Albarzan, J.F.M. Jecong, R. Kurtulus, A.H. Almuqrin, T. Kavas, Investigation of the optical, mechanical, and radiation shielding features for strontium-borotellurite glass system: fabrication, characterization, and EPICS2017 computations, Optik 243 (2021), 167468, https://doi.org/10.1016/j.ijleo.2021.167468.

[20] R. Kurtulus, C. Kurtulus, T. Kavas, Nuclear radiation shielding characteristics and physical, optical, mechanical, and thermal properties of lithium-borotellurite glass doped with Rb2O, Prog. Nucl. Energy 141 (2021), 103961, https://doi.org/10.1016/j.pnucene.2021.103961.

[21] I. Abdullahi, S. Hashim, S.K. Ghoshal, A.U. Ahmad, Structures and spectroscopic characteristics of barium-sulfur-telluro-borate glasses: role of Sm3+ and Dy3+ Co-activation, Mater. Chem. Phys. 247 (2020), 122862, https://doi.org/10.1016/j.matchemphys.2020.122862.

[22] G. Kilic, S.A.M. Issa, E. Ilik, O. Kilicoglu, U.G. Issever, R. El-Mallawany, B. Issa, H.O. Tekin, Physical, thermal, optical, structural and nuclear radiation shielding properties of Sm2O3 reinforced borotellurite glasses, Ceram. Int. 47 (2021) 6154–6168, https://doi.org/10.1016/j.ceramint.2020.10.194.

[23] M. Kamislioglu, Research on the effects of bismuth borate glass system on nuclear radiation shielding parameters, Results Phys. 22 (2021), 103844, https://doi.org/10.1016/j.rinp.2021.103844.

[24] E. Kavaz, E.H. Ghanim, A.S. Abouhaswa, Optical, structural and nuclear radiation security properties of newly fabricated V2O5-SrO-PbO glass system, J. Non-Cryst. Solids 538 (2020), 120045, https://doi.org/10.1016/j.jnoncrysol.2020.120045.

[25] S.A.M. Issa, A. Kumar, M.I. Sayyed, M.G. Dong, Y. Elmahroug, Mechanical and gamma-ray shielding properties of TeO2-ZnO-NiO glasses, Mater. Chem. Phys. 212 (2018) 12–20, https://doi.org/10.1016/j.matchemphys.2018.01.058.

[26] M.I. Sayyed, S.A.M. Issa, H.O. Tekin, Y.B. Saddeek, Comparative study of gamma-ray shielding and elastic properties of BaO–Bi2O3–B2O3 and ZnO–Bi2O3–B2O3 glass systems, Mater. Chem. Phys. 217 (2018) 11–22, https://doi.org/10.1016/j.matchemphys.2018.06.034.

[27] K.A. Naseer, G. Sathiyapriya, K. Marimuthu, T. Piotrowski, M.S. Alqahtani, E.S. Yousef, Optical, elastic, and neutron shielding studies of Nb2O5 varied Dy3+ doped barium-borate glasses, Optik 251 (2022), 168436, https://doi.org/10.1016/j.ijleo.2021.168436.

[28] M.H.A. Mhareb, Physical, optical and shielding features of Li2O−B2O3−MgO−Er2O3 glasses co-doped of Sm2O3, Appl. Phys. A 126 (2020) 71, https://doi.org/10.1007/s00339-019-3262-9.

[29] F.H.F. Al-Saeedi, M.I. Sayyed, F.L. Kapustin, H. Al-Ghamdi, E.V. Kolobkova, O.L. Tashlykov, A.H. Almuqrin, K.A. Mahmoud, A novel barium oxide-based Iraqi sand glass to attenuate the low gamma-ray energies: fabrication, mechanical, and radiation protection capacity evaluation, Nucl. Eng. Technol. 54 (2022) 3051–3058, https://doi.org/10.1016/j.net.2022.03.016.

[30] S. Kaewjaeng, S. Kothan, W. Chaiphaksa, N. Chanthima, R. Rajaramakrishna, H.J. Kim, J. Kaewkhao, High transparency La2O3-CaO-B2O3-SiO2 glass for diagnosis x-rays shielding material application, Radiat. Phys. Chem. 160 (2019) 41–47, https://doi.org/10.1016/j.radphyschem.2019.03.018.

[31] S. Kaewjaeng, N. Chanthima, J. Thongdang, S. Reungsri, S. Kothan, J. Kaewkhao, Synthesis and radiation properties of Li2O-BaO-Bi2O3-P2O5 glasses, Mater. Today Proc. 43 (2021) 2544–2553, https://doi.org/10.1016/j.matpr.2020.04.615.

[32] Y. Al-Hadeethi, M.I. Sayyed, BaO–Li2O–B2O3 glass systems: potential utilization in gamma radiation protection, Prog. Nucl. Energy 129 (2020), 103511, https://doi.org/10.1016/j.pnucene.2020.103511.

[33] N. Chanthima, J. Kaewkhao, P. Limkitjaroenporn, S. Tuscharoen, S. Kothan, M. Tungjai, S. Kaewjaeng, S. Sarachai, P. Limsuwan, Development of BaO−ZnO−B2O3 glasses as a radiation shielding material, Radiat. Phys. Chem. 137 (2017) 72–77, https://doi.org/10.1016/j.radphyschem.2016.03.015.

[34] S. Dubuis, S.H. Messaddeq, Y. Ledemi, A. Côté, Y. Messaddeq, Effect of Bi₂O₃ on the physical, structural and NIR emission properties of BGG glasses prepared using different melting atmospheres, Opt. Mater. Express 11 (2021) 2560, https://doi.org/10.1364/OME.430811.

[35] X.-5M.C. Team, MCNP — A General Monte Carlo N-Particle Transport Code, 2003, Version 5.

[36] A. Kumar, A. Jain, M.I. Sayyed, F. Laariedh, K.A. Mahmoud, J. Nebhen, M.U. Khandaker, M.R.I. Faruque, Tailoring bismuth borate glasses by incorporating PbO/GeO2 for protection against nuclear radiation, Sci. Rep. 11 (2021) 1–14, https://doi.org/10.1038/s41598-021-87256-1.

[37] H.A. Al-Yousef, M. Alotiby, A. Kumar, B.M. Alotaibi, N.A.M. Alsaif, M.I. Sayyed, K.A. Mahmoud, Y. Al-Hadeethi, Physical, structural, and gamma ray shielding studies on novel (35+x) PbO-5TeO2-20Bi2O3-(20-x) MgO-20B2O3 glasses, J. Aust. Ceramic Soc. 57 (2021) 971–981, https://doi.org/10.1007/s41779-021-00600-6.

[38] A.S. Altowyan, A.S. Abouhaswa, M.I. Sayyed, K.A. Mahmoud, Y. Al-Hadeethi, Newly developed glass samples containing P2O5−B2O3−Bi2O3−Li2O−CdO and their performance in optical and radiation attenuation applications, Optik 242 (2021), 167219, https://doi.org/10.1016/j.ijleo.2021.167219.

[39] K.A. Naseer, K. Marimuthu, K.A. Mahmoud, M.I. Sayyed, The concentration

impact of Yb^{3+} on the bismuth boro-phosphate glasses: physical, structural, optical, elastic, and radiation-shielding properties, Radiat. Phys. Chem. 188 (2021), 109617, https://doi.org/10.1016/j.radphyschem.2021.109617.

[40] O.L. Tashlykov, M.I. Sayyed, K.A. Mahmoud, M.U. Khandaker, D.A. Bradley, S.G. Vlasova, Tailor made barium borate doped Bi2O3 glass system for radiological protection, Radiat. Phys. Chem. 187 (2021), 109558, https://doi.org/10.1016/j.radphyschem.2021.109558.

[41] K.A. Naseer, K. Marimuthu, K.A. Mahmoud, M.I. Sayyed, Impact of Bi2O3 modifier concentration on barium−zincborate glasses: physical, structural, elastic, and radiation-shielding properties, Eur. Phy. J. Plus. 136 (2021) 116, https://doi.org/10.1140/epjp/s13360-020-01056-6.